Self-Assembled, 10 nm-Tailored, Near Infrared Plasmonic Metasurface Acting as Broadband Omnidirectional Polarizing Mirror

Esther Soria, Pilar Gomez-rodriguez, Christophe Tromas, Sophie Camelio, David Babonneau, Rosalia Serna, José Gonzalo, Johann Toudert

DOI: 10.1002/ ((please add manuscript number))
Article type: Full Paper

Self-assembled, 10 nm-tailored, near infrared plasmonic metasurface acting as broadband omnidirectional polarizing mirror

Esther Soria, Pilar Gomez, Christophe Tromas, Sophie Camelio, David Babonneau, Rosalía Serna, José Gonzalo, and Johann Toudert**

E. Soria, P. Gomez, Prof. R. Serna, Dr. J. Gonzalo, Dr. J. Toudert
Laser Processing Group, Instituto de Optica, IO-CSIC, Serrano 121, 28006 Madrid, Spain
E-mail: j.gonzalo@io.cfmac.csic.es, johann.toudert@gmail.com

Prof. C. Tromas, Prof. S. Camelio, Dr. D. Babonneau
Institut Pprime, Dept. of Physics and Mechanics of Materials, UPR 3346, CNRS-Université de Poitiers-ENSMA, SP2MI, TSA 41123, 86073 Poitiers Cedex 9, France

Keywords: plasmonics, metasurfaces, self-assembly, metal nanorods, polarization

Abstract. Plasmonic metasurfaces tailored at the few-nm scale and fabricated by high-throughput lithography-free methods are needed to efficiently produce optical components with optimal performance and small footprint. Herein, we report the design of such metasurfaces and their fabrication over cm^2 areas by self-assembly. They present an optical cavity structure, in which a 2D array of parallel Au nanorods is coupled to a metal reflector through a thin spacer. The nanorods present a quasi-monodisperse ~10 nm diameter and separation, and a broad polydisperse length distribution. These outstanding nanostructural features, combining periodicity in one direction with randomness in another, endow the nanorod array with unconventional plasmonic and anisotropic effective optical properties. For light polarized along the nanorods, the metasurface displays strong destructive optical interference and thus near perfect absorption over a broad range of angles of incidence and of wavelengths in the near infrared. In contrast, for light polarized perpendicular to the nanorods, no interference occurs and thus the metasurface behaves as a metal mirror. In sum, the metasurface can be used as broadband omnidirectional polarizing mirror, an original thin and monolithic optical component merging the functionalities of a metal mirror and of a wire-grid polarizer.

1. Introduction

Over the past years, plasmonic metasurfaces have arisen as powerful material platforms for manipulating the spectrum, polarization and topology of optical beams.[1] Accordingly, they have enabled flat and subwavelength-thin optical components such as lenses, beam steerers, phase shifters, coatings with structural colors, polarization controllers or mirrors, opening the way to photonic devices with new functionalities and a smaller footprint.[1-8] To present optimal optical functionalities, the structure of plasmonic metasurfaces must be tailored at a scale much smaller than their operation wavelength. Therefore, for operation in the ultraviolet, visible and near infrared regions, such tailoring must be achieved at the scale of few nm. Such accuracy lies at the limit of the techniques currently employed for plasmonic metasurface fabrication, for instance electron beam lithography or focused ion beam lithography, techniques that in addition suffer from a low fabrication throughput.

In this context, there is a strong demand for developing alternative lithography-free approaches to fabricate plasmonic metasurfaces tailored *at the scale of few nm* for applications in the ultraviolet, visible and near infrared regions. Particularly appealing are self-assembly methods, which enable the accurate fabrication and organization of nanostructures and are excellent for upscaling. Despite of these positive aspects, the potential of these methods for the fabrication of plasmonic metasurfaces tailored at the scale of few nm has been seldom considered.[9-11] Indeed, in most of the works reporting self-assembled plasmonic metasurfaces, the characteristic scale for tailoring lies in the range of few tens of nm.[11-17]

Herein, we report the design and fabrication by a high-throughput self-assembly approach, of plasmonic metasurfaces tailored at the scale of a few nm. They are based on a two-dimensional (2D) array of parallel Au nanorods presenting *a quasi-monodisperse few-nm diameter and separation*, and *a broad polydisperse length distribution in the range from few*

tens of nm to 1 μm. These combined nanostructural features endow the nanorod array with unconventional plasmonic and anisotropic effective optical properties in the near infrared. In this spectral region, no transverse plasmon is excited in the nanorods because of their few-nm diameter. Therefore, the array is transparent to incoming near infrared light when it is polarized perpendicular to the nanorods. In contrast, the array partially absorbs incoming near infrared light when it is polarized parallel to the nanorods. This partially absorbing character is achieved over a broad spectral range thanks to the excitation of longitudinal plasmon resonances at different wavelengths in the nanorods with different lengths, and to the few-nm separation between them.

In the considered metasurfaces, where the nanorod array is incorporated into an optical cavity structure inspired by the "optical Salisbury screen" design,[18] these unconventional plasmonic and anisotropic effective optical properties lead to (i) no destructive optical interference and thus a high, mirror-like reflectance, for the polarization perpendicular to the nanorods; (ii) strong destructive optical interference and thus a near-perfect absorption of light for the polarization parallel to the nanorods.[18-25] The effective optical properties of the nanorod array present a suitable wavelength-dependence to enable such well-contrasted interference and reflection/absorption properties to occur in the near infrared in a broad range of wavelengths and angles of incidence.

This makes the metasurface behave as a broadband omnidirectional polarizing mirror in this spectral region. Such optical component merges, within a thin film, the functionalities of a metal mirror and of a wire-grid polarizer. It reflects the incoming light as efficiently as a metal mirror when it is polarized perpendicular to the nanorods, and near-perfectly absorbs it when it is polarized parallel to them. Such original self-assembled component is useful for lowering the footprint of photonic devices by merging two components into a monolithic one with a subwavelength thickness.

2. Concept

To introduce the key structural elements and working principle of such metasurfaces, we first consider the simplified metasurface design depicted in **figure 1**a. It consists of a periodic 2D array of parallel and monodisperse cylindrical Au nanorods with a few-nm diameter (D) and separation (Λ = D, the same from tip-to-tip and side-to-side), supported on a thin transparent spacer (amorphous aluminum oxide, noted hereafter Al_2O_3) coating a metal reflector (Al). This optical cavity design is inspired by the "optical Salisbury screen" configuration,[18] in which we replaced the top continuous metal film by a nanorod array. We consider the cases in which the metasurface is illuminated at normal incidence, with light polarized either perpendicular to the nanorods ($\perp$) or parallel to them (//).

Figure 1b depicts in a simplified way the key optical features of this metasurface in the near infrared. For the $\perp$ polarization, the nanorod array is transparent to the incoming light, which is thus mainly reflected at the Al reflector ($r \sim r_{Al}$). Therefore, for this polarization the metasurface reflects light as efficiently as a metal mirror. In contrast, for the // polarization, the nanorod array absorbs a fraction of the incoming light. Therefore, the amplitude of the directly reflected wave cannot be neglected versus that of the waves escaping the cavity after multiple internal reflections. If the nanorod array and cavity are properly designed, suitable values of the amplitudes (a) and phases (φ) of these waves can be achieved to enable strong destructive optical interference and thus a near-zero reflectance/near-perfect absorption ($\Sigma a e^{j\varphi} \sim 0$) at selected wavelengths.[20,21]

According to this picture, the key to the polarization-dependent near infrared response of the metasurface is the optical anisotropy of the nanorod array in this spectral region. This anisotropy arises from the excitation of a longitudinal plasmon for the // polarization in the near infrared, while no transverse plasmon can be excited for the $\perp$ polarization in this

spectral region.[27-29] To demonstrate this fact, finite difference time domain (FDTD) simulations were performed. Details about these simulations are given in ref. 26 and Supporting Information S1. The FDTD field maps of the nanorod array displayed in figure 1c demonstrate the excitation of a longitudinal plasmon and no transverse plasmon in the near infrared, for a nanorod length L = 50 nm and D = Λ = 10 nm. A similar trend is observed in the FDTD transmittance spectra of the nanorod array, displayed in figure 1d, which were obtained for different L values (from 50 nm to ∞). For L = 50 nm, the longitudinal plasmon peaks at ~ 950 nm and then it shifts deeper in the infrared as L increases.

These plasmonic properties together with the deep-subwavelength values of D and Λ, make the nanorod array behave as an anisotropic effective layer in the near infrared. The anisotropy is uniaxial with the optical axis oriented parallel to the nanorods. For the ⊥ polarization, because no transverse plasmon is excited in the near infrared, the effective layer is transparent in this spectral region. In contrast, for the // polarization, the excitation of the longitudinal plasmon makes the effective layer present a near infrared optical absorption that depends on the wavelength and nanorod length.

This anisotropy leads to very different optical interference properties and thus very different reflectance spectra of the metasurface in the near infrared for the // and ⊥ polarizations, as shown in figure 1e. For the ⊥ polarization, no interference occurs due to the transparency of the effective layer. Therefore, the metasurface presents a high reflectance that is independent of the wavelength and nanorod length. For the // polarization, the wavelength-dependent and nanorod length-dependent absorption of the effective layer yields interference properties that depend on these two quantities. These trends are seen in figure 1e where the FDTD reflectance of the metasurface is represented for different L values (from 50 nm to ∞). For selected nanorod lengths (50, 100 nm) a band with very low reflectance appears as a result of

strong destructive interference for the // polarization. The position of this band depends on L. However, note that it is not necessarily close to the peak wavelength of the longitudinal plasmon, which may yield to a too strong absorption to enable interference at this wavelength. In Supporting Information S1, it is also shown how the interference properties of the metasurface depend on Λ and on the nanorod cross-section morphology.

These results suggest that a metasurface based on nanorods presenting monodisperse few-nm D and Λ and broadly polydisperse lengths (and thus an inhomogeneously broadened effective longitudinal plasmon absorption[30]) will present, over a broadened range in the near infrared, a high reflectance for the ⊥ polarization and a low reflectance for the // polarization. Let us stress that, to ensure a strong reflectance contrast between the two polarizations, in such metasurfaces the separation between nanorods should remain small. Indeed, increasing much this separation would make the absorption of the effective layer under // polarized light become too low to achieve the balance needed between directly and multiply reflected waves for destructive interference. In that case the reflectance would thus become similar for both polarizations. Keeping the nanorod separation at a small value is also important to ensure that the nanorod array displays an effective behavior. Finally, it is expected that the observed interference phenomena will enable the reflectance of the metasurface to be independent of the angle of incidence, in the same way as in conventional optical Salisbury screens.[21]

Summarizing, metasurfaces with a 2D nanorod array/spacer/reflector structure, where the parallel Au nanorods present a quasi-monodisperse few-nm diameter and separation together with broadly polydisperse lengths, are appealing to achieve broadband omnidirectional polarizing mirrors operating in the near infrared.

3. Results and discussion

3.1. Fabrication of 2D arrays of Au nanorods

As a first step for the fabrication of such metasurfaces, we focused on growing 2D arrays of parallel Au nanorods with a quasi-monodisperse few-nm diameter and separation together with broadly polydisperse lengths. At such aim, Au was deposited at glancing incidence onto periodic nanorippled amorphous aluminum oxide (Al_2O_3) films supported on transparent fused silica substrates,[31] as shown in **figure 2**a. By such means, the Au deposit grows selectively on the ripple sides that face the incoming metal flux, to form parallel Au nanorods whose diameter and separation are driven by the dimensions of the nanoripples.[32] In contrast, there is no geometrical restriction on the nanorod length, which is thus driven by stochastic nucleation-diffusion-growth events. Therefore, while the nanorods grow with a very narrow distribution of diameter and separation distance, their length distribution can be very broad.

The experimental pulsed laser deposition setup used to grow the nanorod arrays is schematized in figure 2b and related experimental details are given in Supporting Information S2. Figure 2b also shows a topographic image typical of the nanorippled Al_2O_3 films used. Herein, we chose nanoripples with a 27 nm period to grow nanorods with a near 10 nm diameter and separation. Parallel nanorods with such small and quasi-monodisperse diameter and separation were successfully grown, as seen in the transmission electron microscopy image shown in figure 2c. In this image, the average values of D, side-to-side separation $\Lambda_{//}$ and tip-to-tip separation $\Lambda_{\perp}$ appear to be 12.6 nm, 15.7 nm, and 8.6 nm, respectively. Figure 2c also confirms the broad length polydispersity of the nanorods. The corresponding length distribution, characterized by digital image analysis (Supporting Information S3), is shown in figure 2d. This distribution spans from a few tens of nm to near one μm, with a maximum near 200 nm.

Note that all these structural features are representative of the whole surface of the grown material, which was deposited homogeneously over a cm^2 area. This homogeneity is seen in the inset of figure 2c, which shows a macroscopic image of a nanorod array sample. The nanorod array absorbs partially visible light and displays a homogeneous grey color over the cm^2 sample area. Such cm^2 scale homogeneity, achieved by a single step process, shows the suitability of our approach to fabricate nanostructure arrays tailored down to the few-nm scale, with a much higher throughput than lithography techniques.

Furthermore, to our knowledge of the literature,[33-49] this is one of the first times that 2D arrays of metal nanorods with such structural features (parallel orientation, few-nm quasi-monodisperse D and Λ, very broad L distribution) are fabricated by self-assembly on a transparent substrate. These previous works relied mainly on approaches such as physical vapor deposition on nanorippled or facetted surfaces,[33-42, 44-47] or by self-ordering of colloids onto wrinkled surfaces.[48,49] As shown in Supporting Information S4, similar features were reported only in refs. 26, 42 and 47.

3.2. Effective optical properties of the 2D arrays of Au nanorods

The outstanding structural features of the fabricated nanorod arrays enable them to present effective optical properties with strong uniaxial anisotropy. To unveil such properties, the transmittance and reflectance of a nanorod array on nanorippled Al_2O_3 film/fused silica were measured in the visible and near infrared, for several angles of incidence and polarizations of the incoming light. The obtained spectra are shown in Supporting Information S5. These spectra were fitted using a layered model depicted in **figure 3**a. In this model, the nanorod array was represented by a uniaxial effective layer presenting a complex refractive index $N_{//} = n_{//} + ik_{//}$ along the nanorods, and a complex refractive index $N_{\perp} = n_{\perp} + ik_{\perp}$ perpendicular to them. These four wavelength-dependent quantities were left free during the fit, which was

realized using the transfer matrix method with mean-square error minimization algorithms. By such means, an excellent fit quality was achieved (Supporting Information S5).

The best fit spectra of $n_{//}$, $k_{//}$, $n_{\perp}$ and $k_{\perp}$ are displayed in figure 3b. They confirm the strong anisotropy and show that, in the near infrared, the effective layer is transparent (resp. partially absorbing) for the ⊥ polarization (resp. // polarization). In addition, it is worth noting that the extinction coefficient $k_{//}$ presents similar spectral features to those of a continuous Au film, yet with lower values and a weaker increase with the wavelength. Correspondingly, when the incoming light is polarized along the nanorods, the nanorod array behaves as a partially absorbing metal film in a broad spectral range. Moreover, as explained hereafter, the wavelength-dependence of $N_{//}$ is suitable for achieving strong destructive interference effects in the cavity structure for a broad range of wavelengths in the near infrared. In contrast, no such strong interference would occur for the incoming light polarized perpendicular to the nanorods in the near infrared.

3.3. Metasurfaces based on the fabricated 2D nanorod arrays

To evaluate the optical properties of metasurfaces based on the fabricated nanorod arrays, we simulated the visible-near infrared reflectance spectra of the design shown in figure 3c, where the wavelength-dependent $n_{//}$, $k_{//}$, $n_{\perp}$ and $k_{\perp}$ of the effective layer were those shown in figure 3b. Simulations were done with the transfer matrix method (necessary details are given in Supporting Information S6). The simulated spectra obtained for different values of the spacer thickness t are shown in figure 3d. For the ⊥ polarization, whereas some oscillations occur in the visible as a result of destructive interference, such interference is absent in the near infrared so that a high reflectance is observed in this spectral region. Remarkably, the reflectance becomes as high as that of an Al mirror (0.93) for wavelengths above 1000 nm if the spacer is thick enough (t = 200 nm). For the // polarization, a low reflectance resulting

from strong destructive interference can be achieved in a broad spectral range in the near infrared if the spacer is thick enough. For t = 200 nm, a reflectance close to 0.3 can be achieved for wavelengths above 1000 nm. Note that these values are lower than expected from the simulations of figure 1. One first reason to that might be that the actual nanorod dimensions and morphology slightly depart from those used in these simulations. This is partly supported by the FDTD simulations shown in Supporting Information S1. A second reason might be that, because each nanorod has a polydisperse environment, it is excited by a near field with different spectral and spatial features compared with that of periodic FDTD models. Such different features would lead to a different excitation of each nanorod, which might support multipole plasmon modes with a broad spectral density (see discussions on polydispersity in ref. 11). A third reason might be that the actual complex refractive index of the Au nanorods differs from those used in these simulations, because of electronic confinement. For t = 300 nm, the additional propagation phase shift brought by the larger spacer thickness enables to achieve even lower reflectance values (less than 0.1) in the C spectral band (1530-1565 nm). With the metasurface structure considered, where light enters through the glass substrate, the reflectance could be further lowered by adding an anti-reflection coating at the air-glass interface.

This shows the potential of our Au nanorod arrays to build metasurfaces acting as efficient polarizing mirrors operating over a broad range in the near infrared. Besides the high near infrared reflectance (comparable to that of an Al mirror) predicted for the $\perp$ polarization, it is especially remarkable that a very low reflectance approaching 0 can be achieved in a broad spectral range in the near infrared for the // polarization. As shown in Supporting Information S6 (figure S6.2), the spectral range in which // polarized reflectance can approach 0 is much broader than for a continuous Au film/Al_2O_3/Al cavity with the same thicknesses. This occurs because the effective optical properties of the nanorod array under this polarization present a

suitable wavelength-dependence to achieve strong interference in a broad spectral range, in contrast with an Au film that absorbs too strongly at long wavelengths. In fact, the capability of the Au nanorod array to enable strong interference for the // polarization in a broad spectral range in the near infrared is comparable with that of Cr films, one of the wisest choices to build broadband near-perfect absorbers.[19,22,23] This is seen by comparing the // polarized reflectance spectrum of the metasurface with that of a continuous Cr film/Al_2O_3/Cr cavity with the same thicknesses (figure S6.2): both present a similarly low reflectance for wavelengths above 1200 nm.

3.4. Fabricated metasurface and its optical properties

To test our theoretical design with experiments, we fabricated a metasurface based on the nanorod array studied above. This metasurface is schematized in **figure 4**a. To produce the depicted structure, an Al_2O_3 spacer with a 190 nm thickness was grown by pulsed laser deposition onto the nanorod array. This spacer was finally covered with a 50 nm-thick Al reflector grown by evaporation. The fabricated metasurface showed a homogeneous visual aspect over a cm^2 area.

The R_p and R_s reflectance spectra of this metasurface measured at near-normal incidence with the plane of incidence perpendicular to the nanorods are shown in figure 4b. In this configuration, R_p (resp. R_s) measurements probe the metasurface with the electric field $\perp$ (resp. //) to the nanorods. The measured spectra show features similar to those predicted by simulations. In particular, in the near infrared they show a high R_p and a low R_s (near 0.3 for a broad range of wavelengths above 1000 nm). A similar strong contrast is observed in a broad range of AOIs, as seen in figure 4c that shows that R_p and R_s remain unchanged upon increasing the incidence angle to 70º. Note that this is true either when the plane of incidence is perpendicular to the nanorods or parallel to them. This confirms the suitability of the

fabricated metasurfaces for acting as broadband omnidirectional polarizing mirror in the infrared.

4. Conclusions and outlook

In summary, we have reported self-assembled plasmonic metasurfaces tailored at the scale of few nm and grown homogeneously over cm^2 scale areas, and we have demonstrated the suitability of such metasurfaces for achieving an original thin and monolithic optical component. In particular, we considered metasurfaces with a 2D Au nanorod array/Al_2O_3 spacer/Al reflector cavity structure, where the nanorods present a parallel orientation, a quasi-monodisperse few-nm diameter and separation, and a broad polydisperse length distribution. These outstanding nanostructural features were achieved by growing the nanorods by pulsed laser deposition at glancing angle onto periodic nanorippled Al_2O_3 substrates. They endow the nanorod array with unconventional plasmonic and anisotropic effective optical properties enabling the metasurface to behave as a broadband omnidirectional polarizing mirror in the near infrared.

In this spectral region, no transverse plasmon is excited so that the array is transparent to light polarized perpendicular to the nanorods. This leads to the absence of destructive optical interference within the metasurface, which therefore reflects light with this polarization as efficiently as an Al mirror. In contrast, for light polarized parallel to the nanorods, multiple longitudinal plasmons are excited within the array at different wavelengths in the near infrared. Therefore, in this spectral region, the array absorbs light partially and the wavelength dependence of its effective optical properties lead to strong destructive interference within the metasurface over a broad range of wavelengths. This enables the metasurface to display a near-perfect absorption of near infrared light when it is polarized parallel to the nanorods, with a performance comparable to that of continuous Cr film/Al_2O_3 spacer/Al reflector cavity

structures, one of the wisest choices to achieve broadband near-perfect absorption in the near infrared.

To our knowledge, this is the first time that a self-assembled metamaterial design harnesses nanoscale monodispersity/periodicity in one direction and nanoscale polydispersity/randomness in another direction to achieve in a broad spectral range no interference for one polarization and strong interference for the other. Indeed, in recent literature, although nanostructuration and randomness have been considered to achieve strong interference in a broad spectral range, this was done without considering or harnessing anisotropy effects.[11,18, 22-25]

Note that, while in this work we grew Au nanorods with a near 10 nm diameter and separation, the nanorod dimensions could be even more finely tuned to further enhance the metamaterial optical properties. Such fine tuning can be achieved for instance by depositing the Au onto nanorippled substrates with a different period. Furthermore, the proposed metasurface concept can also be implemented using other materials than Au, for instance Ag and Al, to achieve polarizing mirrors operating in other spectral regions, such as the visible or ultraviolet.

Supporting Information

Supporting Information is available from the Wiley Online Library or from the author.
S1. Details about FDTD simulations; S2. Details about the metasurface fabrication; S3. Digital image analysis of the nanorod array; S4. Self-assembled 2D arrays of parallel metal nanostructures: literature data; S5. Reflectance and transmittance spectra of the nanorod array; S6. Simulation of the metasurface reflectance spectra.

Acknowledgements

Lamellae for TEM analysis were prepared at the “Laboratorio de Microscopías Avanzadas” (Instituto de Nanociencia de Aragón-Universidad de Zaragoza). Authors acknowledge L. Casado and I. Rivas for their preparation. TEM analysis was conducted at the National Center for Electronic Microscopy (Universidad Complutense de Madrid). Dr. J. Garcia and Dr. J. de la Portilla are acknowledged for his support in the TEM analysis and the binarization of TEM images, respectively. Dr. J.I. Larruquert is acknowledged for the deposition of the Al reflector. This research was funded by the Spanish Research Agency (AEI, Ministry of Research and Innovation) and the European Regional Development Fund (ERDF) under grant RTI 2018-

096498-B-I00. The work of P. Gomez was supported by the Autonomous Community of Madrid and the European Social Fund (contract E-28-2019-0767805).

Received: ((will be filled in by the editorial staff))
Revised: ((will be filled in by the editorial staff))
Published online: ((will be filled in by the editorial staff))

References

[1] P. Genevet, F. Capasso, F. Aieta, M. Khorasaninejad, R. Devlin, *Optica* **2017**, *4*, 1, 139-152.

[2] Y. Kim, P.C. Wu, R. Sokhoyan, K. Mauser, R. Glaudell, G.K. Shirmanesh, H.A. Atwater, *Nano Lett.* **2019**, *19*, 6, 3961-3968.

[3] J. Sung, G.-Y. Lee, B. Lee, *Nanophotonics* **2019**, *8*, 10, 1701-1718.

[4] M. Song, D. Wang, S. Peana, S. Choudhury, P. Nyga, Z.A. Kudyshev, H. Yu, A. Boltasseva, V.M. Shalaev, A.V. Kildishev, *Appl. Phys. Rev.* **2019**, *6*, 041308.

[5] F. Ding, R. Deshpande, S.I. Bozhevolnyi, *Light: Science and Applications* **2018**, *7*, 17178.

[6] A. Basiri, X. Chen, J. Bai, P. Amrollahi, J. Carpenter, Z. Holman, C. Wang, Y. Yao, *Light: Science and Applications* **2019**, *8*, 78.

[7] S. De Zuani, M. Rommel, B. Gompf, A. Berrier, J. Weis, M. Dressel, *ACS Photon.* **2016**, *3*, 1109-1115.

[8] S. Xiao, H. Mühlenbernd, G. Li, M. Kenney, F. Liu, T. Zentgraf, S. Zhang, J. Li, *Adv. Opt. Mater.* **2016**, *4*, 654-658.

[9] Q. Shi, T. U. Connell, Q. Xiao, A.S.R. Chesman, W. Cheng, A. Roberts, T.J. Davis, D.E. Gómez, *ACS Photon.* **2019**, *6*, 314-321.

[10] S. Wang, F. Chen, R. Ji, M. Hou, F. Yi, W. Zheng, T. Zhang, W. Lu, *Adv. Opt. Mater.* **2019**, *7*, 1801596.

[11] J. Toudert, *Phys. Status Solidi A* **2019**, 1900677.

[12] M. Mayer, M.J. Schnepf, T.A.F. König, A. Fery, *Adv. Opt. Mater.* **2019**, *7*, 1800564.

[13] L. Malassis, P. Massé, M. Tréguer-Delapierre, S. Mornet, P. Weisbecker, P. Barois, C.R. Simovski, V.G. Kravets, A.N. Grigorenko, *Adv. Mater.* **2014**, *26*, 324-330.

[14] F. Ligmajer, L. Kejík, U. Tiwari, M. Qiu, J. Nag, M. Konecny, T. Sikola, W. Jin, R.F. Haglund, Jr., K. Appavoo, D.Y. Lei, *ACS Photon.* **2018**, *5*, 2561-2567.

[15] S.D. Golze, R.A. Hughes, S. Rouvimov, R.D. Neal, T.B. Demille, S. Neretina, *Nano Lett.* **2019**, *19*, 5633-5660.

[16] B. Liu, S. Chen, J. Zhang, X. Yao, J. Zhong, H. Lin, T. Huang, Z. Yang, J. Zhu, S. Liu, C. Lienau, L. Wang, B. Ren, *Adv. Mater.* **2018**, *30*, 1706031.

[17] G. Baraldi, M. García Pardo, J. Gonzalo, R. Serna, J. Toudert, *Adv. Mater. Interfaces* **2018**, *5*, 1800241.

[18] J. Nath, E. Smith, D. Maukonen, R.E. Peale, *J. Appl. Phys.* **2014**, *115*, 19, 193103.

[19] H. Deng, Z. Li, L. Stan, D. Rosenman, D. Czaplewski, J. Gao, X. Yang, *Opt. Lett.* **2015**, *40*, 11, 2592-2595.

[20] M.A. Kats, F. Capasso, *Laser Photonics Rev.* **2016**, *10*, 5, 735-749.

[21] J. Toudert, R. Serna, M. García Pardo, N. Ramos, R.J. Peláez, B. Maté, *Opt. Express* **2018**, *26*, 26, 34043-34059.

[22] A. Ghobadi, H. Hajian, B. Butun, E. Ozbay, *ACS Photon.* **2018**, *5*, 11, 4203-4221.

[23] A. Ghobadi, H. Hajian, A.R. Rashed, B. Butun, E. Ozbay, *Photon. Res.* **2018**, *6*, 3, 168-176.

[24] G.-H. Jung, S. Yoo, J.-S. Kim, Q.-H. Park, *Adv. Opt. Mater.* **2019**, *7*, 7, 1801229.

[25] D.U. Yildirim, A. Ghobadi, M.C. Soydan, O. Atesal, A. Toprak, M.D. Caliskan, E. Ozbay, *ACS Photon.* **2019**, *6*, 1812-1822.

[26] J. Toudert, R. Serna, C. Deeb, E. Rebollar, *Opt. Mater. Express* **2019**, *9*, 7, 2924-2936.

[27] V. Myroshnychenko, J. Rodríguez-Fernández, I. Pastoriza-Santos, A.M. Funston, C. Novo, L.M. Liz-Marzán, F.J. García de Abajo, *Chem. Soc. Rev.* **2008**, *37*, 9, 1792-1805.

[28] B.N. Khlebtsov, N.G. Khlebtsov, *J. Phys. Chem. C* **2007**, *111*, 11516-11527.

[29] K.-S. Lee, M.A. El-Sayed, *J. Phys. Chem. B* **2005**, *109*, 20331-20338.

[30] A. Resano-Garcia, Y. Battie, A. En Naciri, S. Akil, N. Chaoui, *J. Chem. Phys.* **2015**, *142*, 134108.

[31] D. Babonneau, E. Vandenhecke, S. Camelio, *Phys. Rev. B* **2017**, *95*, 085412.

[32] S. Camelio, E. Vandenhecke, S. Rousselet, D. Babonneau, *Nanotechnology* **2014**, *25*, 3, 035706.

[33] S. Camelio, D. Babonneau, D. Lantiat, L. Simonot, F. Pailloux, *Phys. Rev. B* **2009**, *80*, 155434.

[34] D. Babonneau, S. Camelio, L. Simonot, F. Pailloux, P. Guérin, B. Lamongie, O. Lyon, *Europhys. Lett.* **2011**, *93*, 26005.

[35] M. Garel, D. Babonneau, A. Boulle, F. Pailloux, A. Coati, Y. Garreau, A.Y. Ramos, H.C.N. Tolentino, *Nanoscale* **2015**, *7*, 1437-1445.

[36] S. Yazidi, A. Fafin, S. Rousselet, F. Pailloux, S. Camelio, D. Babonneau, *Phys. Status Solidi C* **2015**, *12*, 12, 1344-1348.

[37] R. Verre, K. Fleischer, C. Smith, N. McAlinden, J.F. McGilp, I.V. Shvets, *Phys. Rev. B* **2011**, *84*, 085440.

[38] R. Verre, K. Fleischer, O. Ualibek, I.V. Shvets, *Appl. Phys. Lett.* **2012**, *100*, 031102.

[39] L. Anghinolfi, R. Moroni, L. Mattera, M. Canepa, F. Bisio, *J. Phys. Chem. C* **2011**, *115*, 14036-14043.

[40] L. Anghinolfi, L. Mattera, M. Canepa, F. Bisio, *Phys. Rev. B* **2012**, *85*, 235426.

[41] G. Maidecchi, G. Gonella, R.P. Zaccaria, R. Moroni, L. Anghinolfi, A. Giglia, S. Nannarone, L. Mattera, H.-L. Dai, M. Canepa, F. Bisio, *ACS Nano* **2013**, *7*, 7, 5834-5841.

[42] A. Toma, D. Chiappe, D. Massabò, C. Boragno, F. Buatier de Mongeot, *Appl. Phys. Lett.* **2008**, *93*, 163104.

[43] A. Toma, D. Chiappe, C. Boragno, F. Buatier de Mongeot, *Phys. Rev. B* **2010**, *81*, 165436.

[44] T.W.H. Oates, A. Keller, S. Noda, S. Facsko, *Appl. Phys. Lett.* **2008**, *93*, 063106.

[45] M. Ranjan, T.W.H. Oates, S. Facsko, W. Möller, *Opt. Lett.* **2010**, *35*, 15, 2576-2578.

[46] M. Ranjan, S. Facsko, *Nanotechnology* **2012,** *23*, 48, 485307.

[47] Q. Jia, M. Langer, B. Schreiber, J. Grenzer, P.F. Siles, R.D. Rodriguez, K. Huang, Y. Yuan, A. Heidarian, R. Hübner, T. You, W. Yu, K. Lenz, J. Lindner, X. Wang, S. Facsko, *Nano Res.* **2018**, *11*, 3519-3528.

[48] C. Hanske, M. Tebbe, C. Kuttner, V. Bieber, V.V. Tsukruk, M. Chanana, T.A.F. König, A. Fery, *Nano Lett.* **2014**, *14*, 6863-6871.

[49] M. Tebbe, M. Mayer, B.A. Glatz, C. Hanske, P.T. Probst, M.B. Müller, M. Karg, M. Chanana, T.A.F. König, C. Kuttner, A. Fery, *Faraday Discuss.* **2015**, *181*, 243-260.

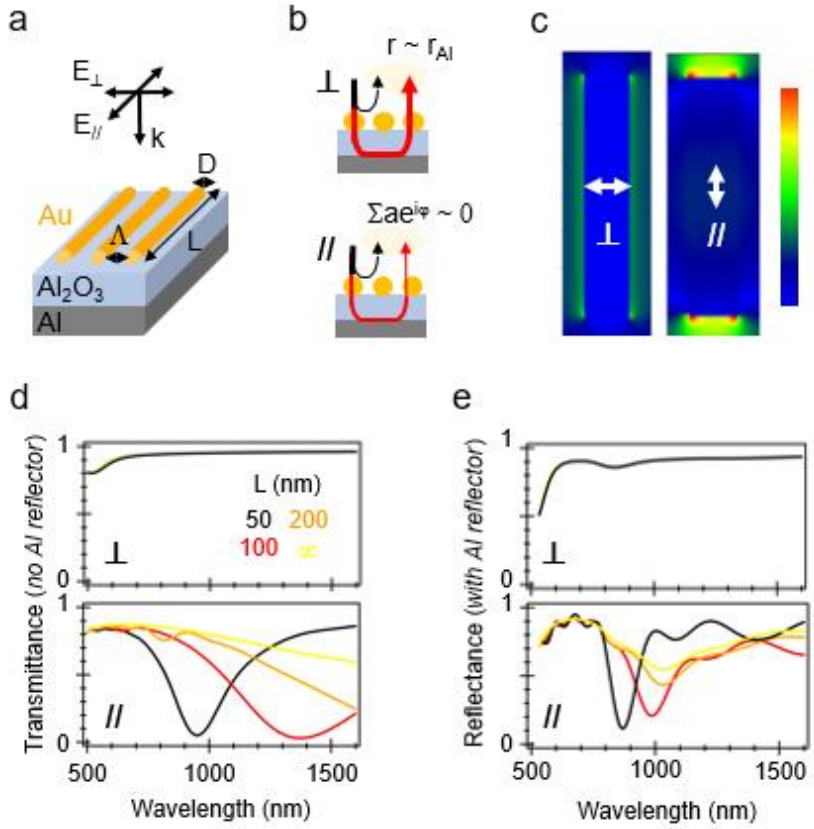

Figure 1. Metasurface based on a 2D array of parallel Au nanorods: working principle. (a) Simplified metasurface design considered as example. The nanorods are cylindrical, monodisperse (length L, diameter D), parallel and organized on a periodic array. They are separated from tip-to-tip and side-to-side by the same distance Λ. They lie on an Al_2O_3 spacer coating an Al reflector. (b) Simplified representation of the key optical features of the metasurface in the near infrared, for the polarization of the incoming light ⊥ and // to the nanorods. The black arrow represents the directly reflected wave, and the red arrow represents the wave escaping after being reflected once by the Al reflector. (c) FDTD-simulated near-field maps of a unit cell of the metasurface at normal incidence, for the ⊥ and // polarization. The wavelength was 860 nm, and we took L = 50 nm, D = Λ = 10 nm and thicknesses of 200 nm and 50 nm for the spacer and reflector, respectively. The map is observed in the equatorial plane of the nanorod array. The color scale ranges from 0 to 4 (resp. 0 to 15) for the ⊥ (resp. //) polarization. (d) FDTD-simulated transmittance spectra of the nanorod array (for these simulations, the Al reflector was removed). (e) FDTD-simulated reflectance spectra of the metasurface. In (d) and (e) the spectra were simulated for different values of L.

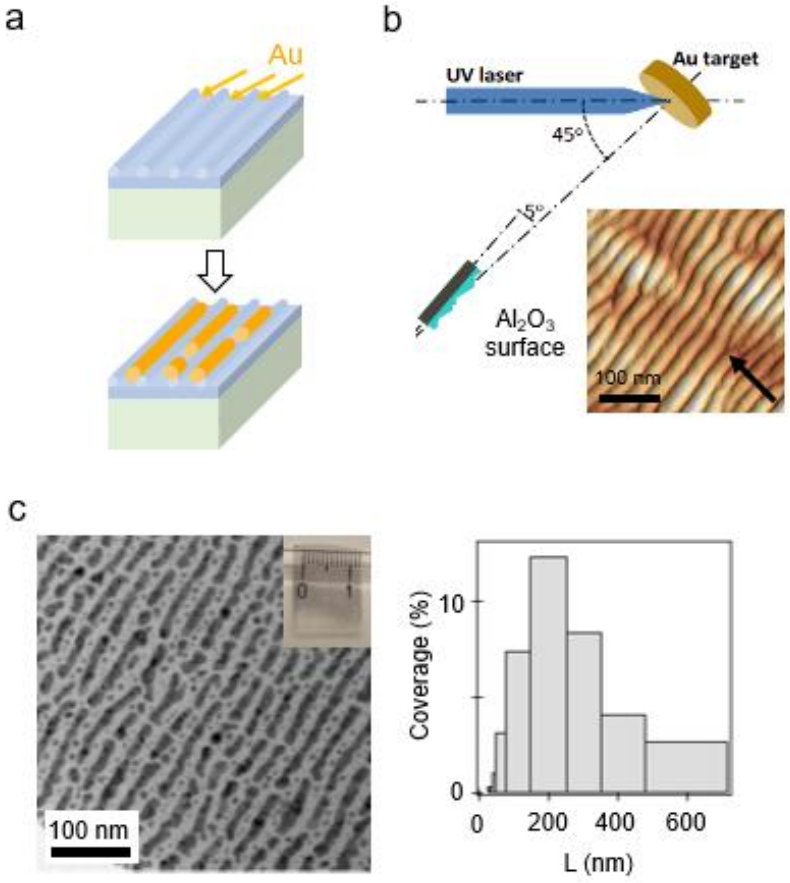

Figure 2. Fabrication of 2D arrays of Au nanorods. (a) Schematic representation of the glancing incidence deposition process of Au onto a nanorippled Al_2O_3 film to form the nanorods. The nanorippled Al_2O_3 film is supported on a transparent fused silica substrate. (b) Geometry of the setup used for Au deposition, and topographic image (atomic force microscopy) of a nanorippled Al_2O_3 film. The black arrow represents the direction of the incident Au atoms. A corresponding height profile is shown in Supporting Information S2.1. (c) Top-view transmission electron microscopy image of a 2D array of Au nanorods grown onto nanorippled Al_2O_3. Inset: Macroscopic image of a nanorod array sample taken with a digital camera. (c) Distribution of the nanorod length L.

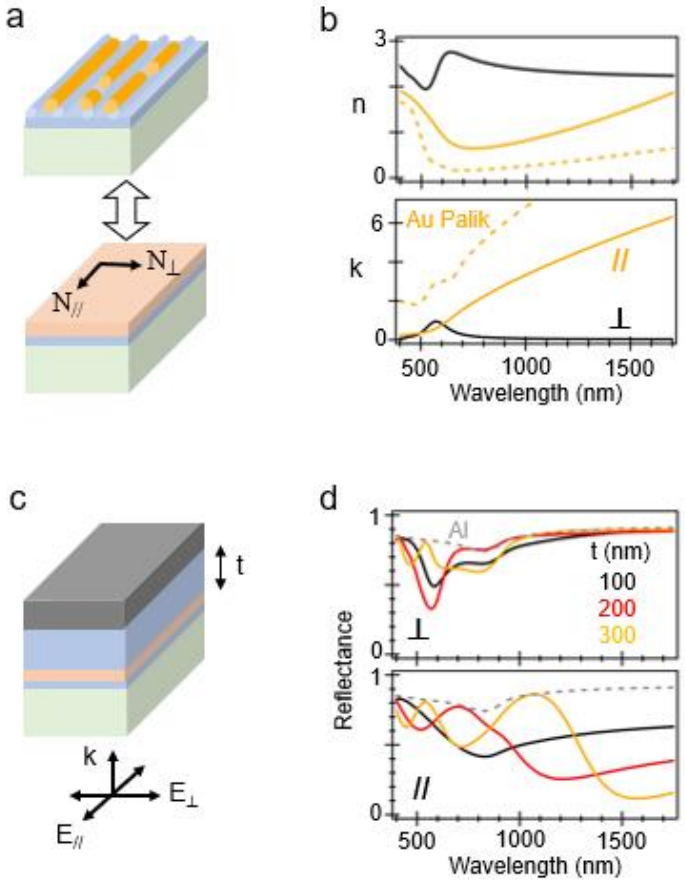

Figure 3. Effective optical properties of the fabricated 2D arrays of Au nanorods and their relevance for the design of metasurfaces acting as polarizing mirror. (a) Layered model used for determining the complex effective refractive index of the nanorod array, parallel and perpendicular to the nanorods ($N_{//}$ and $N_{\perp}$). The effective layer accounting for the nanorod array is shown in pink. Its thickness was set to 10 nm. The Al_2O_3 thickness was set to 40 nm. (b) Measured best fit spectra of the real part n and imaginary part k of these complex refractive indices (solid lines). The n and k spectra of Au from the Palik database are shown for comparison (dotted lines). (c) Structure of a metasurface incorporating this effective layer. It is covered by an Al_2O_3 spacer with thickness t and a 50 nm-thick Al reflector. Light is shined onto the metasurface through the transparent fused silica substrate. (d) Transfer matrix-simulated reflectance spectra of this metasurface at normal incidence, for the // and ⊥ polarizations, as a function of the spacer thickness. In the simulations, the complex refractive indices shown in (b) were used for the effective layer. The simulated reflectance spectrum of an Al mirror is shown for comparison.

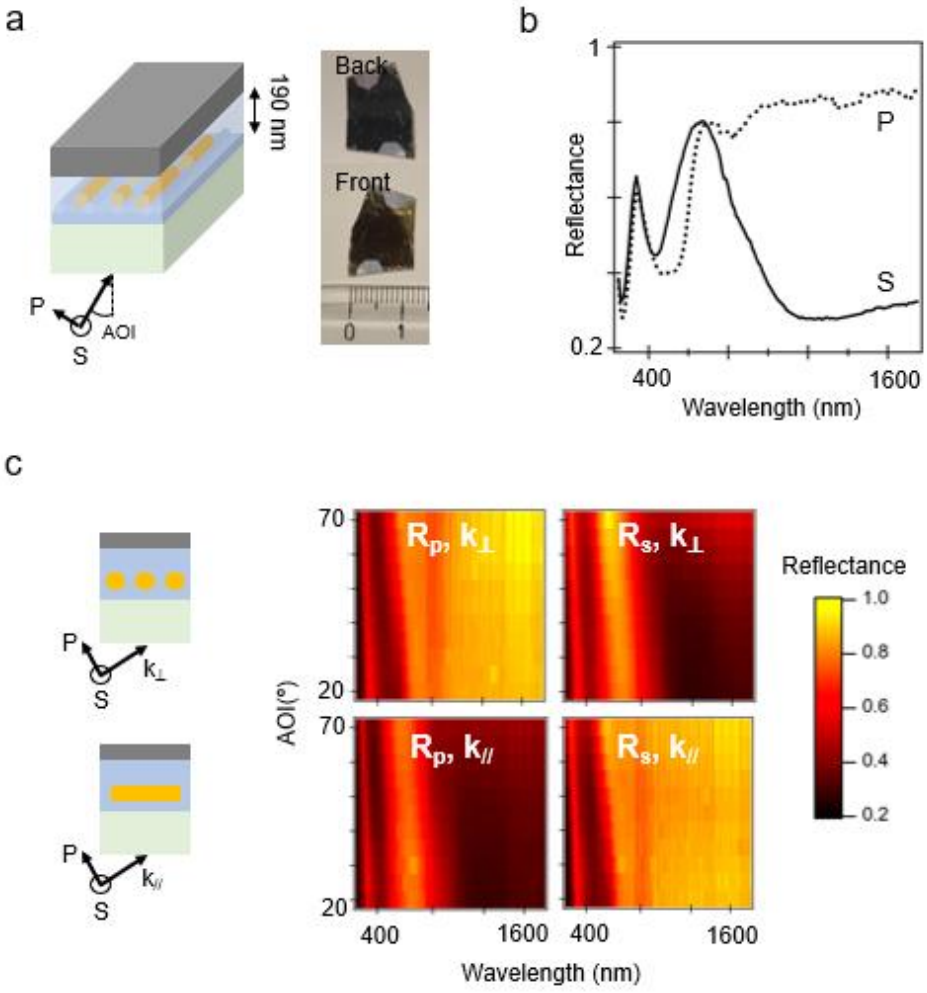

Figure 4. Structure and optical properties of the fabricated Au nanorod array-based metasurface. (a) Schematic representation of the metasurface structure. The nanorod array is covered by a 190 nm-thick Al_2O_3 spacer and a 50 nm thick Al mirror. Macroscopic images of a metasurface sample taken with a digital camera, from the glass side (front) and from the reflector side (back). (b) Measured reflectance spectra of this metasurface at near normal incidence (angle of incidence AOI of 20º, plane of incidence perpendicular to the nanorods), for S (solid line, equivalent to //) and P (dotted line, equivalent to ⊥) polarizations. (c) Maps of the reflectance of this metasurface versus wavelength and AOI, for the plane of incidence perpendicular ($k_\perp$) and parallel ($k_{//}$) to the nanorods, and for S and P polarized light.

Self-assembled plasmonic metasurfaces tailored down to 10 nm are reported. They combine non-conventional in-plane structural features (randomness along one direction and periodicity along the other) with a vertical resonant cavity design. This enables them to behave as broadband coherent near-perfect absorber for one polarization and high-quality mirror for the other. Therefore, they can be used as broadband omnidirectional polarizing mirror.

Self-assembled plasmonic metasurfaces

Esther Soria, Pilar Gomez, Christophe Tromas, Sophie Camelio, David Babonneau, Rosalía Serna, José Gonzalo, and Johann Toudert**

Self-assembled, 10 nm-tailored, near infrared plasmonic metasurface acting as broadband omnidirectional polarizing mirror